BRAIN
A JOURNAL OF NEUROLOGY

Glymphatic MRI in idiopathic normal pressure hydrocephalus

Geir Ringstad,[1,2] Svein Are Sirirud Vatnehol[3] and Per Kristian Eide[2,4]

The glymphatic system has in previous studies been shown as fundamental to clearance of waste metabolites from the brain interstitial space, and is proposed to be instrumental in normal ageing and brain pathology such as Alzheimer's disease and brain trauma. Assessment of glymphatic function using magnetic resonance imaging with intrathecal contrast agent as a cerebrospinal fluid tracer has so far been limited to rodents. We aimed to image cerebrospinal fluid flow characteristics and glymphatic function in humans, and applied the methodology in a prospective study of 15 idiopathic normal pressure hydrocephalus patients (mean age 71.3 ± 8.1 years, three female and 12 male) and eight reference subjects (mean age $41.1 + 13.0$ years, six female and two male) with suspected cerebrospinal fluid leakage (seven) and intracranial cyst (one). The imaging protocol included T_1-weighted magnetic resonance imaging with equal sequence parameters before and at multiple time points through 24 h after intrathecal injection of the contrast agent gadobutrol at the lumbar level. All study subjects were kept in the supine position between examinations during the first day. Gadobutrol enhancement was measured at all imaging time points from regions of interest placed at predefined locations in brain parenchyma, the subarachnoid and intraventricular space, and inside the sagittal sinus. Parameters demonstrating gadobutrol enhancement and clearance in different locations were compared between idiopathic normal pressure hydrocephalus and reference subjects. A characteristic flow pattern in idiopathic normal hydrocephalus was ventricular reflux of gadobutrol from the subarachnoid space followed by transependymal gadobutrol migration. At the brain surfaces, gadobutrol propagated antegradely along large leptomeningeal arteries in all study subjects, and preceded glymphatic enhancement in adjacent brain tissue, indicating a pivotal role of intracranial pulsations for glymphatic function. In idiopathic normal pressure hydrocephalus, we found delayed enhancement ($P < 0.05$) and decreased clearance of gadobutrol ($P < 0.05$) at the Sylvian fissure. Parenchymal (glymphatic) enhancement peaked overnight in both study groups, possibly indicating a crucial role of sleep, and was larger in normal pressure hydrocephalus patients ($P < 0.05$ at inferior frontal gyrus). We interpret decreased gadobutrol clearance from the subarachnoid space, along with persisting enhancement in brain parenchyma, as signs of reduced glymphatic clearance in idiopathic normal hydrocephalus, and hypothesize that reduced glymphatic function is instrumental for dementia in this disease. The study shows promise for glymphatic magnetic resonance imaging as a method to assess human brain metabolic function and renders a potential for contrast enhanced brain extravascular space imaging.

1 Department of Radiology and Nuclear Medicine, Oslo University Hospital, Rikshospitalet, Oslo, Norway
2 Faculty of Medicine, University of Oslo, Oslo, Norway
3 The Intervention Centre, Oslo University Hospital-Rikshospitalet, Oslo, Norway
4 Department of Neurosurgery, Oslo University Hospital-Rikshospitalet, Oslo, Norway

Correspondence to: Professor Per Kristian Eide, MD PhD
Department of Neurosurgery
Oslo University Hospital – Rikshospitalet
Pb 4950 Nydalen
N-0424 Oslo, Norway
E-mail: p.k.eide@medisin.uio.no or peide@ous-hf.no

Introduction

The 'glymphatic' (glia-lymphatic) system denotes a brain-wide pathway for clearance of brain metabolites, and depends on convective fluid transport through the interstitial space, mediated by AQP4 channels at astrocytic perivascular end feet (Iliff *et al.*, 2012). Impaired glymphatic transport with accumulation of cellular waste products such as amyloid-β and tau aggregation has been proposed as instrumental in conditions such as normal ageing (Kress *et al.*, 2014), brain trauma (Plog *et al.*, 2015) and Alzheimer's disease (Iliff *et al.*, 2012). Glymphatic transport of solutes is highly dependent on sleep (Xie *et al.*, 2013) and body posture (Lee *et al.*, 2015).

While studies of the mouse brain have applied two-photon *in vivo* imaging, assessment of glymphatic function has been performed with MRI in rat brain, using subarachnoid administration of the linear, gadolinium-based contrast agent Gd-DTPA (gadolinium-diethylenetriaminpentaacetate) (Iliff *et al.*, 2013a; Yang *et al.*, 2013). Gd-DTPA is of small molecular weight (938 Da), which is an important precondition for access of solutes to the interstitial space (Iliff *et al.*, 2012). Gd-based contrast agents have already been used to some extent to diagnose CSF leaks as cause of intracranial hypotension in humans, and been documented to have low risk (Jinkins *et al.*, 2002; Reiche *et al.*, 2002; Aydin *et al.*, 2004; Akbar *et al.*, 2012). By administration of an intrathecal contrast agent at the lumbar level, 'glymphatic MRI' may thereby bridge the gap from animal studies to investigations of glymphatic clearance of solutes from the human brain interstitial space (Jessen *et al.*, 2015). A case report demonstrated, for the first time, signs of glymphatic contrast enhancement in a patient under clinical work-up for CSF leakage (Eide and Ringstad, 2015); however, no patient cohort has yet been investigated with glymphatic MRI.

Glymphatic convective solute transport through the interstitial space is dependent on arterial pulsations (Iliff *et al.*, 2013b). Impaired glymphatic function may therefore be a factor in poorly understood diseases characterized by reduced intracranial compliance and thus restricted intracranial artery pulsations, such as in idiopathic normal pressure hydrocephalus (iNPH) (Eide and Sorteberg, 2010). INPH is a neurodegenerative disease with a typical symptom triad of gait ataxia, urinary incontinence and dementia and can be treated surgically with CSF diversion procedures (Adams *et al.*, 1965). Altered glymphatic function in iNPH could possibly be a mechanism behind the high comorbidity between iNPH and Alzheimer's disease (Cabral *et al.*, 2011).

The purpose of this study was therefore to assess CSF flow characteristics and glymphatic function in a cohort of patients with iNPH and reference subjects with MRI before and at multiple time points after intrathecal contrast agent administration.

Materials and methods

The study was approved by the Institutional Review Board (2015/1868), Regional Ethics Committee (2015/96) and the National Medicines Agency (15/04932-7). Inclusion was by written and oral informed consent.

Experimental design

In this prospective, observational study, consecutive patients with iNPH and reference subjects were imaged with MRI before, and at multiple time points (10 min to 24 h) after intrathecal lumbar administration of the MRI contrast agent gadobutrol. Patients with iNPH and reference subjects were prospectively enrolled from October 2015 to May 2016. After gadobutrol administration, all patients and reference subjects were admitted and observed in the hospital for at least 24 h. Exclusion criteria were: history of hypersensitivity reactions to contrast agents; history of severe allergy reactions in general, evidence of renal dysfunction, pregnant or breastfeeding females, and age < 18 or > 80 years.

According to the observational study design, randomization of patients was not relevant, neither was *a priori* sample size calculations. As ventricular enlargement is inherent with the iNPH diagnosis, image post-processing could therefore not be done blinded for the dichotomy iNPH/non-iNPH.

Subjects

Patients with idiopathic normal pressure hydrocephalus

We included consecutive iNPH patients who were referred to the Department of Neurosurgery, Oslo University Hospital - Rikshospitalet, Oslo, Norway based on clinical symptoms and findings indicative of iNPH, and with imaging findings of ventriculomegaly. Within the Department of Neurosurgery, a clinical assessment was done, and clinical severity graded based on a previously described NPH grading scale (Eide and Sorteberg, 2010). All patients underwent overnight intracranial pressure monitoring for the purpose of selection for shunt surgery by using threshold levels as previously defined (Eide and Sorteberg, 2010).

Reference subjects

Reference subjects were, in parallel with iNPH patients, recruited prospectively and consecutively from referrals to clinical work-up of suspected CSF leakage syndrome or intracranial cysts. They underwent MRI with intrathecal gadobutrol with the primary indication to define site of CSF leakage, or cyst enhancement, respectively.

MRI protocol

Sagittal 3D T_1-weighted volume scans were obtained exclusively in a 3 T Philips Ingenia MRI scanner (Philips Medical systems) with equal imaging protocol settings at all time points. The main imaging parameters were: repetition time = 'shortest' (typically 5.1 ms), echo time = 'shortest' (typically 2.3 ms), flip angle = 8°, field of view = 256×256 cm and matrix = 256×256 pixels (reconstructed 512×512). We sampled 184 over-contiguous (overlapping) slices with 1-mm thickness, which was automatically reconstructed to 368 slices. The total duration of each image acquisition was 6 min and 29 s. At each time point, an automated anatomy recognition protocol based on landmark detection in MRI data (SmartExam^{TM}, Philips Medical Systems) was applied to secure consistency and reproducibility of the MRI studies.

Before gadobutrol administration, we also scanned patients and reference subjects with a sagittal 3D fluid attenuated inversion recovery (FLAIR) volume sequence, where the main imaging parameters were: repetition time = 4800 ms, echo time = 'shortest' (typically 318 ms), inversion recovery time = 1650 ms, field of view = 250×250 mm and matrix = 250×250 pixels (reconstructed 512×512). We sampled 184 over-contiguous slices with 1 mm thickness, which was automatically reconstructed to 365 slices.

Intrathecal administration of gadobutrol

The study participants met at 8 am for a pre-contrast MRI and were thereafter transported on a mobile table to an adjacent neurological surgery room, where an interventional neuroradiologist performed X-ray guided lumbar puncture. Intrathecal injection of 0.5 ml of 1.0 mmol/ml gadobutrol (Gadovist^{TM}, Bayer Pharma) was preceded by verifying the correct position of the syringe tip in the subarachnoid space in terms of CSF backflow from the puncture needle, and by injecting a small amount (typically 3 ml) of 270 mg I/ml iodixanol (Visipaque^{TM}, GE Healthcare) to confirm unrestricted distribution of radiopaque contrast agent in the lumbar subarachnoid space. Following needle removal, the study subjects were instructed to rotate themselves around the long axis of the body once before transportation back to the MRI suite, while remaining in the supine position.

Post-contrast MRI acquisitions

Consecutive, identical MRI examinations with the previously outlined MRI protocol parameters were initiated as soon as possible after intrathecal gadobutrol administration (typically with ~10-min delay), and performed approximately every 10 min during the first hour after contrast agent injection. The study participants were thereafter instructed to remain supine in bed, while one pillow under the head was allowed. Repeated, identical image acquisitions were then performed approximately every 2 h after intrathecal gadobutrol administration until ~4 pm. All transfer of study subjects between the neurosurgical department and the MRI suite, and between the bed and the MRI table, was performed by the hospital staff to allow for the patient to remain in the supine position. The final MRI scanning was performed the next morning (~24 h after contrast agent injection). Patients and controls were allowed to move without any restrictions between the 4 pm examination at the end of Day 1 and the 24 h scan the next morning.

While the MRI exams, for practical reasons, could not be obtained at identical time points for every study subject, all exams were categorized into the following time intervals: pre-contrast, 0–20 min, 20–40 min, 40–60 min, 1–2 h, 2–4 h, 4–6 h, 6–9 h, and 24 h.

Image analysis

For each time point, a neuroradiologist (G.R.) with 10 years' experience in neuroradiology, placed circular regions of interest at predefined locations directly on axially reconstructed T_1-weighted images in the hospital PACS (picture archiving and communication system (Sectra IDS7®, Sectra). Each region of interest provides the mean signal unit from the image grey-scale, which can be compared between time points and study subjects when all MRI sequence parameters are kept equal. All regions of interest were fitted to local anatomy to avoid partial volume effects from neighbouring tissue or CSF. As this human CSF tracer study is conceptually preceded by a similar study in rodents only (Iliff *et al.*, 2013*a*), the position of regions of interest were partly founded on observations made in animals, but also from previously recognized CSF flow patterns in iNPH derived from other sorts of imaging studies such as radionuclide cisternography (Heinz *et al.*, 1970) and phase-contrast MRI (Penn *et al.*, 2011; Ringstad *et al.*, 2016).

For the ventricular and subarachnoid CSF spaces, a single region of interest was placed at the third and fourth ventricle, pontine cistern, and at the foramen magnum (cisterna magna). Bilateral regions of interest were placed inside the frontal horns of the lateral ventricles, Sylvian fissures, and in the central sulci at the vertex of the brain. In addition, perivascular gadobutrol enhancement along the anterior, middle and posterior cerebral arteries at the brain surface was dichotomized as present and non-present, and the time point where such perivascular enhancement could be observed, was registered.

For the brain parenchyma, a single region of interest was placed in the central pons and bilaterally in thalami, inferior frontal gyri anterior to the Sylvian fissures, periventricular white matter outside the frontal horns, and precentral gyri, respectively.

A single region of interest was also placed in the posterior part of the superior sagittal sinus.

Supplementary Fig. 1 illustrates region of interest measurements from the Sylvian fissures and inferior frontal gyri in a patient.

Finally, periventricular hyperintensity detected as any periventricular signal increase on FLAIR images was classified into four grades according to a modification (Iwamoto *et al.*, 2001) of the classification by van Swieten *et al.* (1990): grade 0, no periventricular hyperintensity; grade 1, marginal periventricular hyperintensity; grade 2, moderate between grade 1 and 3; grade 3, severe periventricular hyperintensity extending to the subcortex.

Parameters derived from gadobutrol enhancement

For the enhancement phase, we calculated the time to peak enhancement, maximum change in signal unit, and the enhancement coefficient (signal unit/min) for all regions of interest within the CSF, venous space and brain parenchyma.

For the same regions, we also assessed the signal unit decline from maximum to minimum (latest) enhancement (clearance time), maximum decline in signal units and the clearance coefficient (signal unit/min).

Statistical analysis

Statistical analyses were performed using the SPSS software version 22 (IBM Corporation). Differences between categorical data were determined using Pearson chi-square test, and differences between continuous data were determined using independent samples *t*-tests. Statistical significance was accepted at the 0.05 level (two-tailed).

Results

Patients

Demographic data are presented in Supplementary Table 1. The study includes 15 patients with iNPH and eight reference subjects. The reference subjects underwent MRI due to suspicion of intracranial hypotension associated with CSF leakage ($n = 7$), and one had headache possibly associated with a pineal gland cyst. The patient cohorts were significantly different in terms of age and distribution of symptoms ($P < 0.001$).

In the iNPH cohort, indication for shunt surgery was found in 15/15 patients. In 2/15 patients, shunt surgery was not recommended because of other co-morbidity, and thus 13/15 patients were shunted. All shunted patients (13/13) responded with clinical improvement (Supplementary Table 1).

In the reference subject cohort, one individual (1/8) was treated surgically for a pineal cyst with a good surgical result and subsequent symptom improvement. CSF leakage was found in 2/7 reference subjects (reference Subjects 4 and 5; Fig. 1B), and a dura leak was confirmed during surgery in both. One patient with suspected leakage (reference Subject 1) also underwent intracranial pressure monitoring, which demonstrated normal values.

There were no serious adverse events to gadobutrol administration, either at the lumbar injection site, or systemically. One patient suffered a pulmonary embolism after 1 day; we considered the association with contrast agent administration as unlikely and rather due to a train journey of several hours the day preceding the MRI study.

Distribution of gadobutrol within subarachnoid and ventricular CSF spaces

Delayed CSF enhancement in idiopathic normal pressure hydrocephalus

Figure 1 exemplifies time-dependent distribution of intrathecally administered gadobutrol in a patient with iNPH (Fig. 1A) and a reference subject (Fig. 1B).

Figure 2 provides graphic illustrations (trend plots) of gadobutrol enhancement at different locations in the subarachnoid space and ventricular space.

In patients with iNPH, contrast enhancement was delayed in extra-parenchymal subarachnoid space locations such as CSF in foramen magnum (Fig. 2A), pontine cistern (Fig. 2B), and Sylvian fissure (Fig. 2C). Table 1 provides evidence that time to peak enhancement within the CSF spaces was prolonged, and enhancement thus delayed, in iNPH patients. This was significant for Sylvian fissure (close to inferior frontal gyrus) ($P < 0.05$) and at the vertex of the brain (precentral sulcus) ($P < 0.01$). In iNPH, there was also a trend towards delayed enhancement at the foramen magnum, pontine cistern and Sylvian fissure, but this did not reach statistical significance.

No differences between groups were seen for maximum signal unit increase in subarachnoid space at the foramen magnum, pontine cistern, Sylvian fissure, or over vertex. For the latter, enhancement of gadobutrol was low in both groups within the CSF in the precentral sulci. In 3/15 patients with iNPH and 3/8 reference subjects, gadobutrol enhancement was not detected at the upper convexity of the brain (precentral sulci) at any time points.

Delayed periarterial enhancement in idiopathic normal pressure hydrocephalus

At the outer surface of the brain, gadobutrol distributed uniformly, and mainly along the outside of the anterior, middle and posterior cerebral arteries in all iNPH patients and reference subjects; however, this peri-arterial enhancement pattern was observed to be significantly delayed in patients with iNPH (Fig. 3).

Ventricular reflux in idiopathic normal pressure hydrocephalus

Evidence of ventricular reflux in iNPH was indicated by larger contrast enhancement within the CSF of the fourth ventricle (Fig. 2E), third ventricle (Fig. 2F) and lateral ventricles (Fig. 2G). Moreover, the maximum increase in signal unit was significantly higher within the fourth ($P < 0.05$), third ($P < 0.05$) and lateral ($P < 0.01$) ventricles of iNPH patients, indicating redistribution of CSF to the ventricular spaces in iNPH (Table 1).

Gadobutrol enhancement within brain parenchyma

Glymphatic enhancement dependent of gadobutrol in nearby CSF

Supplementary Table 2 presents T_1 signal before gadobutrol as well as the maximum increase in signal unit after gadobutrol for all individual patients. All individuals demonstrated the presence of brain parenchymal gadobutrol enhancement. An increase of signal unit $\geqslant 10\%$ was observed at all locations (pons: 10/15 iNPH patients, 2/8 reference subjects; thalamus: 12/15 iNPH patients, 3/8
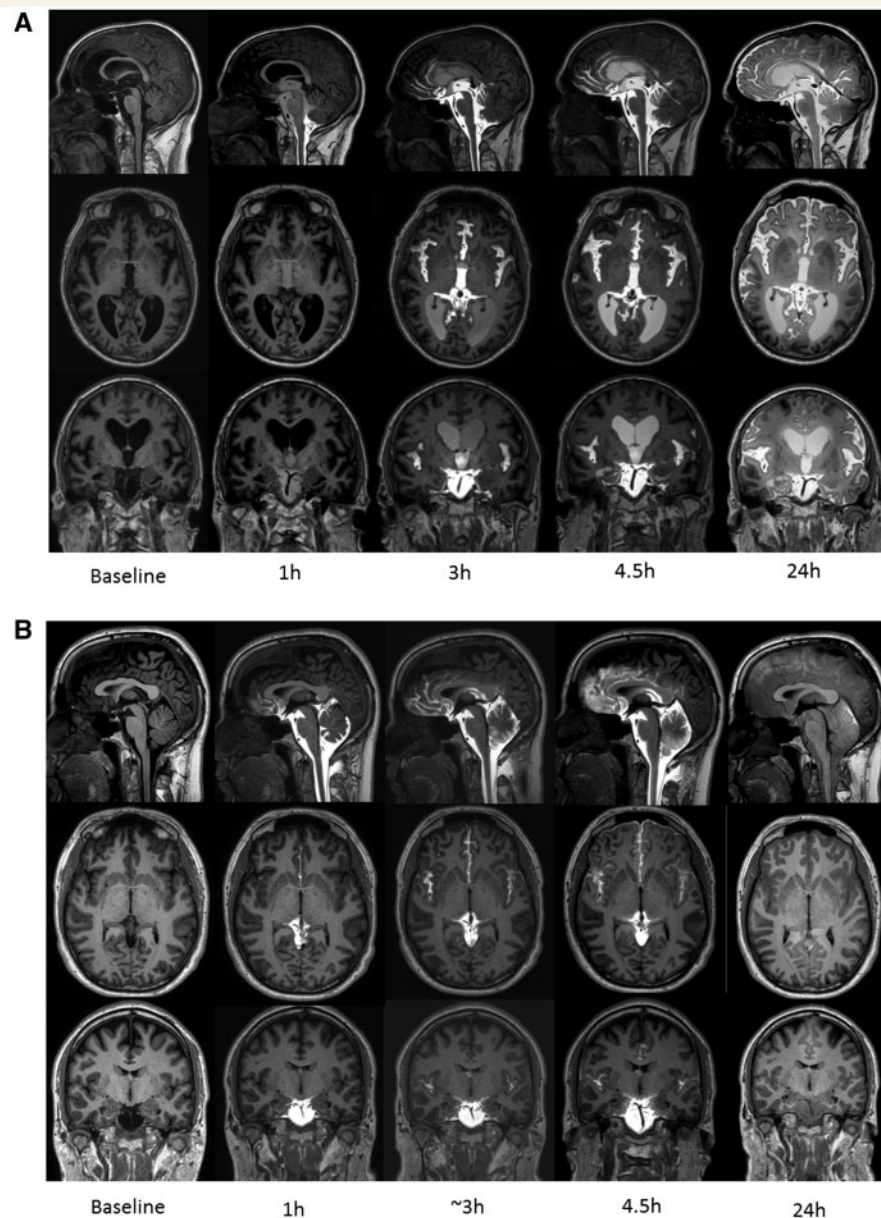
Figure 1 CSF contrast enhancement at multiple time points. Reconstructed T_1-weighted images in sagittal (*top row*), axial (*middle row*) and coronal (*bottom row*) planes from MRI at baseline (before contrast agent administration) and at four of the subsequent imaging time points demonstrating time-dependent contrast enhancement of subarachnoid and intraventricular spaces in iNPH patient (**A**) and reference subject (**B**). Reflux of gadobutrol to the lateral ventricles was a typical feature of iNPH. In **B**, retrodural contrast enhancement can be seen on sagittal images (*top row*) at time points 1 h, 3 h and 4.5 h as sign of a CSF leakage (reference Subject 5).

reference subjects; periventricular frontal horn: 14/15 iNPH patients, 2/8 reference subjects; inferior frontal gyrus: 14/15 iNPH patients, 6/8 reference subjects; precentral gyrus: 5/15 iNPH patients, 2/8 reference subjects). There were interindividual differences. The proportion of patients with $\geqslant 10\%$ increase of signal unit was higher in the iNPH cohort. The change in signal unit depended highly on location, and with the most evident signal unit change at the periventricular white matter of iNPH patients and at the inferior frontal gyrus of iNPH and reference subjects.

Figure 4 demonstrates change in T_1 signal (signal unit) after intrathecal gadobutrol within brain parenchyma at the group level in iNPH patients and reference subjects.

The brain parenchymal contrast enhancement underneath the brain surface correlated with the contrast available in the nearby CSF; Fig. 5 demonstrates maximum increase in signal unit within parenchyma as related to nearby CSF. At the outer surface of the brain, this association was by far strongest between the Sylvian fissure and adjacent inferior frontal gyrus.
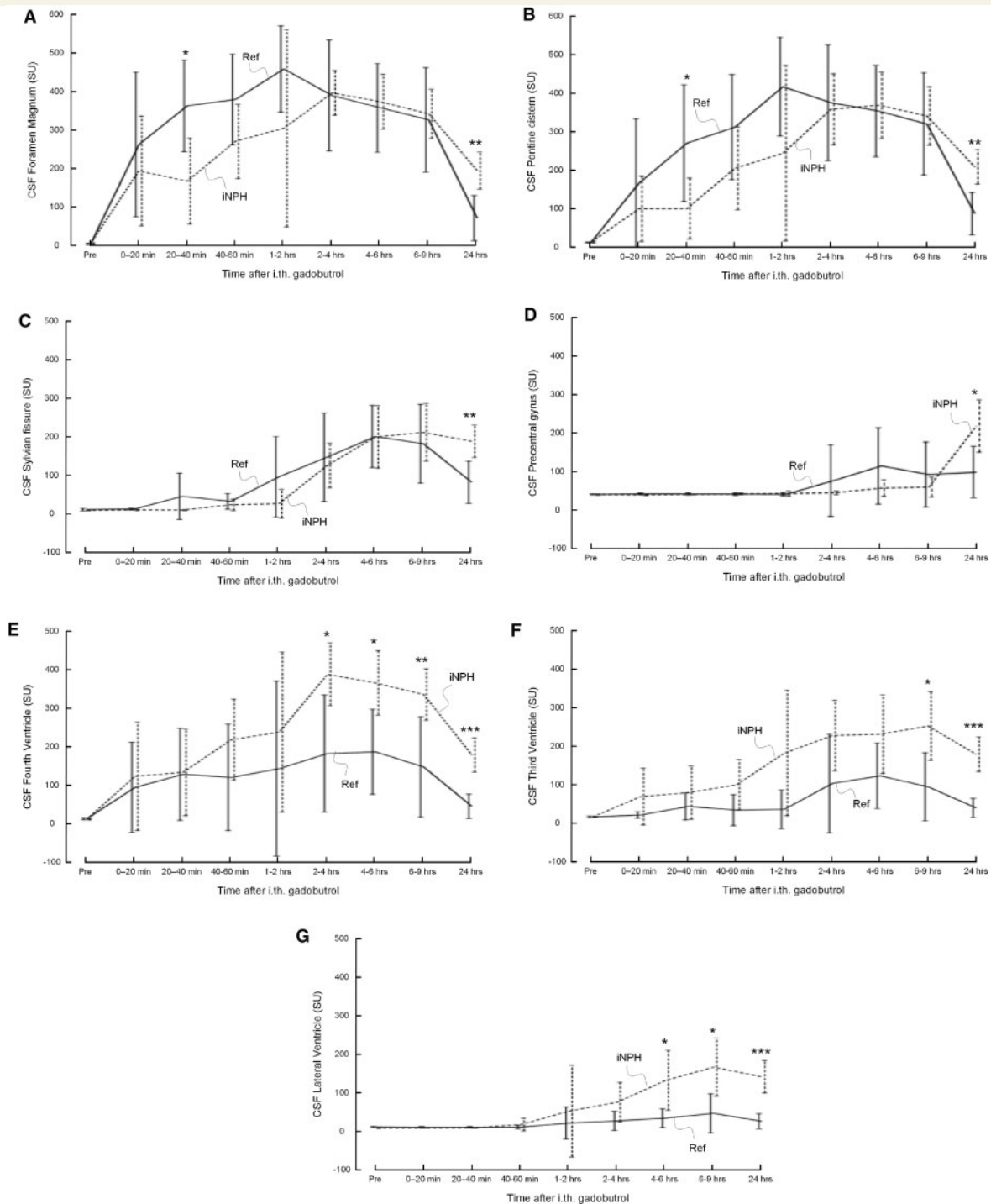
Figure 2 Trend plots of CSF tracer (gadobutrol) enhancement depending on location. Gadobutrol enhancement was delayed in iNPH patients as compared to reference subjects in (**A**) foramen magnum, (**B**) nearby pons, (**C**) Sylvian fissure, and (**D**) precentral sulcus. On the other hand, enhancement was significantly stronger within CSF of (**E**) fourth ventricle, (**F**) third ventricle, and (**G**) lateral ventricles. Reference subjects: continuous lines; iNPH patients: dotted lines. Differences between groups at individual time points were determined by independent samples *t*-test ($*P < 0.05$, $**P < 0.01$, $***P < 0.001$).

Before gadobutrol administration, the parenchymal T_1 signal was significantly lower within iNPH cases in pons, thalamus, periventricular frontal horn, and inferior frontal gyrus, and remained lower at all time points during Day 1

(Fig. 4 and Table 2). Overnight, at 24 h, the T_1 signal had increased in all study subjects, but significantly more in iNPH patients than reference patients as compared to the 4 pm scan in the inferior frontal gyrus ($P < 0.05$) and

Table I Information about the enhancement phase for different regions of interest within CSF and venous space and brain parenchyma

Enhancement phase	Baseline (SU)		Max increase (SU)		Time to peak (min)		Enhancement coefficient (SU/min)	
	iNPH	REF	iNPH	REF	iNPH	REF	iNPH	REF
CSF space								
Foramen magnum	10.3 + 3.4	8.9 + 2.6	398.3 ± 108.0	426.0 ± 123.0	174.5 ± 94.2	129.4 ± 156.7	5.9 ± 12.2	17.7 ± 24.5
Sylvian fissure	7.0 + 1.6	8.6 + 3.6	226.2 ± 100.2	204.2 ± 104.4	689.0 ± 536.3[a]	258.6 ± 114.8	0.57 ± 0.41	0.9 ± 0.7
Pontine cistern	10.2 + 3.7	9.5 + 1.3	378.2 ± 133.0	388.5 ± 121.7	230.9 ± 98.4	159.8 ± 148.9	2.4 ± 2.3	10.8 ± 18.2
Fourth ventricle	11.3 + 3.1	12.6 + 3.0	386.5 ± 138.2[a]	236.0 ± 142.9	286.7 ± 322.9	123.4 ± 98.1	5.6 ± 14.5	6.3 ± 14.0
Third ventricle	14.4 + 2.6	14.5 + 2.8	243.6 ± 136.9[a]	115.1 ± 103.8	615.3 ± 587.5	253.8 ± 133.2	1.4 ± 1.7	0.4 ± 0.4
Lateral ventricle	6.0 + 1.2[c]	9.4 + 1.5	168.5 ± 99.8[b]	42.5 ± 51.9	843.4 ± 560.2	402.6 ± 446.1	0.41 ± 0.39	0.13 ± 0.16
Precentral sulcus	7.6 + 1.6	8.1 + 1.2	131.1 ± 94.1	87.8 ± 99.3	1254.7 ± 483.8[b]	475.0 ± 601.9	0.10 ± 0.06	0.29 ± 0.39
Central venous space								
Sagittal sinus/confluence	34.9 + 7.2	32.3 + 7.6	8.1 ± 8.0	7.4 ± 9.6	350.2 ± 457.3	524.4 ± 591.3	0.16 ± 0.25	0.41 ± 0.85
Brain parenchyma								
Inferior frontal gyrus	82.5 + 4.3[b]	89.5 + 3.2	39.1 ± 25.3	23.8 ± 20.9	1358.0 ± 313.4	1421.3 ± 53.1	0.03 ± 0.02	0.02 ± 0.02
Pons	96.8 + 4.2[a]	101.1 + 4.8	11.6 ± 7.0	7.4 ± 5.8	1090.0 ± 602.3	929.4 ± 676.9	0.03 ± 0.08	0.08 ± 0.17
Thalamus	86.7 + 4.8[b]	93.9 + 6.0	13.0 ± 6.8	9.0 ± 7.1	1261.7 ± 462.6	1288.4 ± 386.3	0.01 ± 0.02	0.01 ± 0.01
Frontal horn	63.9 + 18.4[b]	94.1 + 15.7	48.5 ± 32.8[b]	7.9 ± 7.9	1349.3 ± 350.9	1109.8 ± 585.6	0.04 ± 0.02	0.05 ± 0.12
Precentral gyrus	82.7 + 6.0	87.4 + 3.7	9.0 ± 8.3	7.8 ± 11.2	900.0 ± 686.4	742.8 ± 727.9	0.04 ± 0.06	0.03 ± 0.03

Significant differences between iNPH and REF groups were determined by independent samples t-test: [a]$P < 0.05$, [b]$P < 0.01$, [c]$P < 0.001$.
REF = reference subject; SU = signal unit.

outside the frontal horn ($P = 0.008$) (Supplementary Table 3). Associations between enhancement in CSF and nearby parenchyma were also largest in these locations (R = 0.85, $P < 0.001$ and R = 0.84, $P < 0.001$, respectively).

Transependymal CSF flow in idiopathic normal pressure hydrocephalus

Figure 4C demonstrates contrast enhancement within periventricular white matter parenchyma outside the frontal horns of the lateral ventricles. This enhancement was strongly associated with ventricular reflux of contrast media in the lateral ventricles (Fig. 5D) and significantly higher in iNPH cases (Table 2 and Fig. 2 E–G).

As illustrated in Fig. 6, the present data provide evidence that periventricular hyperintensity on FLAIR images is dependent on transependymal water flux from ventricles to the periventricular white matter. The degree of periventricular hyperintensity, graded 0–3, was significantly related to the contrast enhancement in the periventricular frontal brain parenchyma. The maximum signal unit increase in periventricular frontal brain parenchyma was significantly higher in grade 2 ($P = 0.02$) and grade 3 ($P = 0.03$), as compared to grade 0 (Fig. 6).

Gadobutrol enhancement within central venous space

There was no significant signal unit increase that could be observed in the superior sagittal sinus at any time point after intrathecal administration of gadobutrol, and thus no evidence of any contribution to parenchymal signal unit change from circulating contrast agent in cerebral vessels (Table 2).

Clearance of gadobutrol

At 24 h, contrast enhancement was more profound in all CSF compartments in iNPH patients, which indicates delayed clearance of gadobutrol compared with reference subjects (Fig. 2). This is further detailed in Table 2. Accordingly, the maximum reduction of signal unit was significantly lower within the CSF of foramen magnum ($P < 0.01$), Sylvian fissure ($P < 0.05$) and pontine cistern ($P < 0.01$) in iNPH. The clearance coefficients were significantly lower for iNPH cases within CSF of foramen magnum ($P < 0.01$), Sylvian fissure ($P < 0.05$) and pontine cistern ($P < 0.01$) (Table 2).

For the brain parenchyma, signal unit peaked at 24 h, and the current observation period was therefore too short to determine clearance time of gadobutrol from the brain.

Moreover, and as already noted, there were no signs of gadobutrol enhancement in the central venous space, and therefore estimation of gadobutrol clearance to venous blood was not relevant.

Discussion

In this study, humans (patients with iNPH and reference subjects) were for the first time investigated by use of an intrathecally administered, small molecular weight contrast
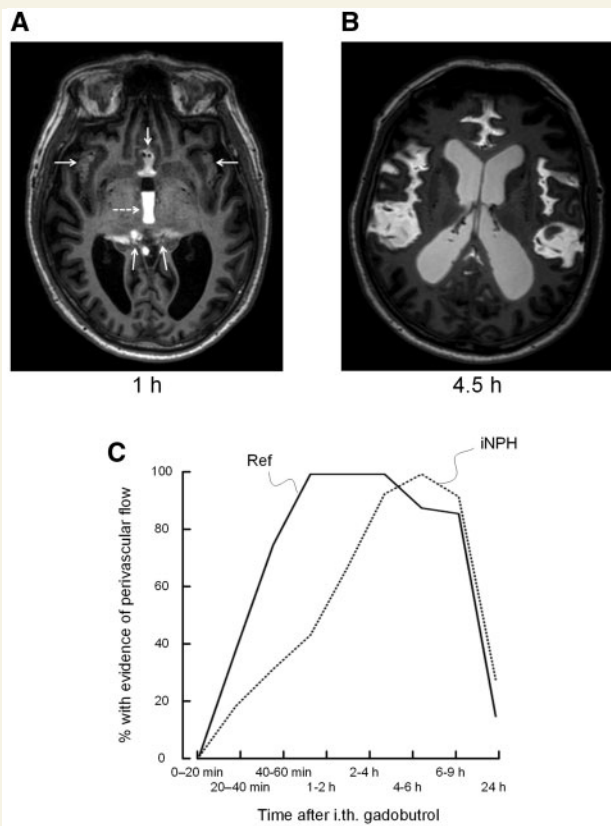
Figure 3 Perivascular enhancement. Gadobutrol enhancement in sulci traversed by the major cerebral arteries (anterior, middle and posterior) was identified and categorized as present/absent for each time point. (**A**) MRI in axial plane 1 h after contrast agent administration shows gadobutrol distributed to the interhemispheric fissure, Sylvian fissure and ambient cistern (arrows), and reflux to the third ventricle (dotted arrow). (**B**) At later time points, even though contrast subsequently distributed more freely in the subarachnoid spaces, there was a clear tendency for enhancement in cerebral fissures traversed by the anterior, middle and posterior arteries in both iNPH and reference subjects. (**C**) Evidence of perivascular gadolinium enhancement was categorized as present/absent for each time point. The percentage of individuals in whom a perivascular contrast enhancement was visualized, is plotted for each time point, showing significant differences between reference subjects and iNPH cohorts (20–40 min: $P = 0.049$; 40–60 min: $P = 0.01$; Pearson chi-square test). The plot in **C** suggests delayed perivascular flow at the brain surface in iNPH patients.

agent (gadobutrol) as CSF tracer to assess brain glymphatic function with MRI (glymphatic MRI) and also CSF flow characteristics in the subarachnoid space and ventricles over multiple time points. The iNPH cohort consisted of a high proportion of 'true', or definitive, iNPH defined by the shunt response rate. Moreover, the reference patients can be considered suitable to serve as controls, as CSF leakage was found in only 2/8. Since intrathecal administration of MRI contrast agent is merely used off-label on clinical indication, inclusion of non-symptomatic controls at this stage of research was not done due to ethical

concerns. Our observations demonstrate that gadobutrol propagates in subarachnoid space antegradely along the outside of large leptomeningeal arteries, and that presence of gadobutrol in subarachnoid space is a prerequisite for glymphatic contrast agent enhancement in adjacent brain parenchyma. Glymphatic enhancement was different between patients and brain regions, occurred much later in humans than reported in rats, and peaked at the final 24 h MRI exam. Clearance of gadobutrol was delayed in iNPH. Moreover, signs of net CSF ventricular reflux and transependymal flow from the ventricles towards periventricular white matter was a characteristic feature of iNPH. Enhancement of gadobutrol outside the upper brain convexities was sparse in both iNPH as well as reference subjects, even after 24 h, and in some subjects was not detectable.

Intrathecal administration of gadobutrol as CSF tracer

The macrocyclic MRI contrast agent gadobutrol has low molecular weight (605 Da) and is a highly hydrophilic, non-ionic compound that easily distributes in water (Cheng, 2004) and is thus well suited as a CSF tracer. While a linear contrast agent (Gd-DTPA) was applied in a previous study of glymphatic function in rat brain (Iliff *et al.*, 2013*a*), it has recently been recommended that consideration should be made in terms of using macrocyclic Gd-based contrast agents rather than linear agents in humans (Malayeri *et al.*, 2016), due to their superior stability in biological tissue (Lohrke *et al.*, 2016). Regarding glymphatic transport, gadobutrol also has the advantages of even smaller molecular size (molecular weight 604 Da) than Gd-DTPA, and higher T_1 relaxation (Lohrke *et al.*, 2016).

In studies of mice (Iliff *et al.*, 2012; Bedussi *et al.*, 2017), tracer has been injected into the cisterna magna at rates and volumes that potentially could overwhelm the intracranial compartment (Hladky and Barrand, 2014), and thereby interfere with physiological CSF flow. Another study has, however, demonstrated that a minor and transient increase in intracranial pressure is unlikely to affect glymphatic tracer transport (Yang *et al.*, 2013). In this study of humans, we injected less than a total of 5 ml fluid into the subarachnoid space, level with the lumbar spine, and interference with intracranial pressure and CSF flow at later time points should therefore be negligible.

In accordance with previous studies using other MRI contrast agents for intrathecal use, gadobutrol also seemed safe for this purpose, as there were no observed serious adverse events related to the administration of contrast agent in the current study groups.

CSF flow characteristics

First signs of gadobutrol at the level of the foramen magnum occurred typically within 20 min for most study subjects, who all were kept in supine position during and
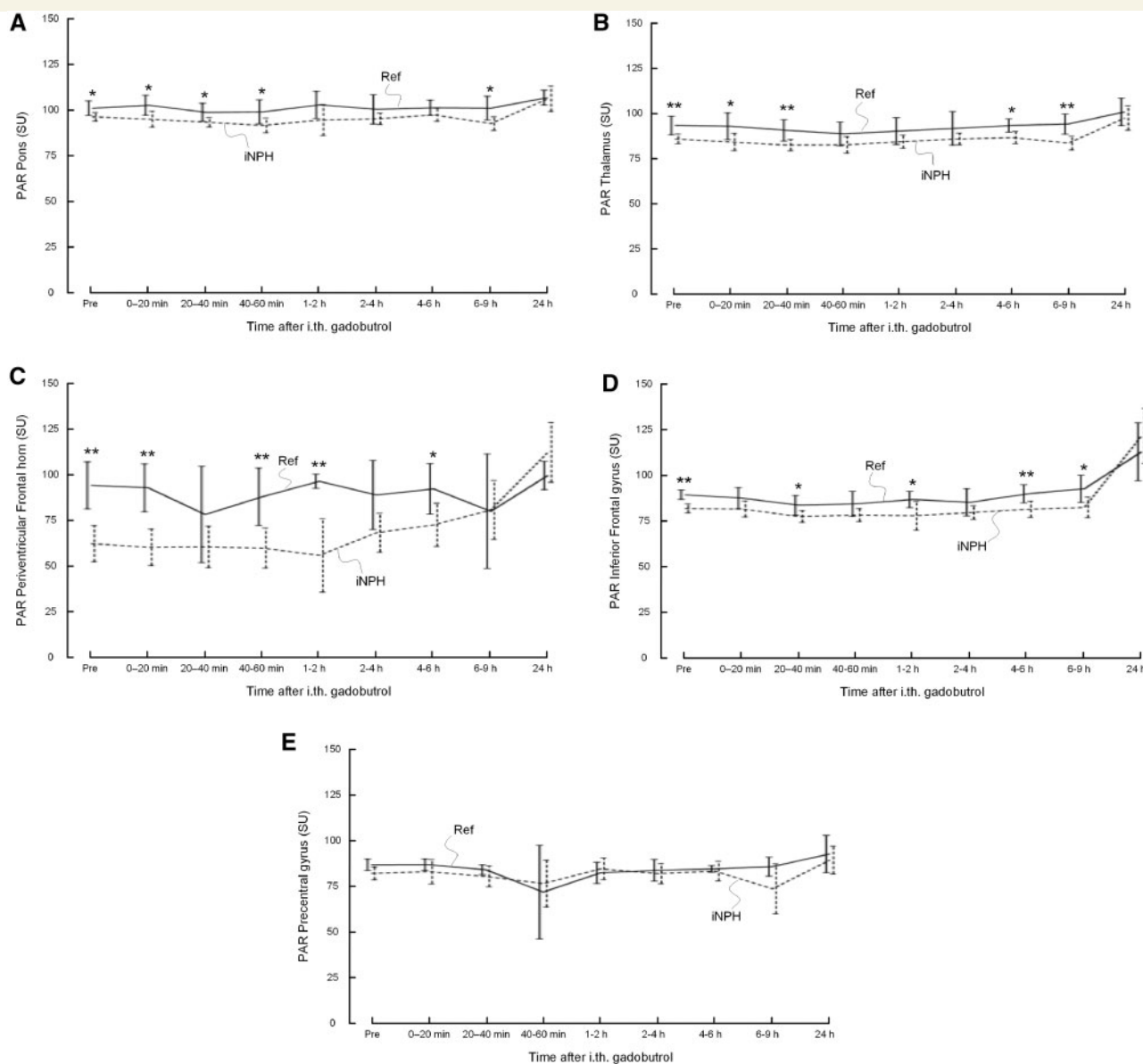
Figure 4 Glymphatic enhancement. Trend plots of gadobutrol enhancement in parenchyma depending on location, including (**A**) pons, (**B**) thalamus, (**C**) periventricular frontal horn, (**D**) inferior frontal gyrus (IFG), and (**E**) precentral gyrus. The T_1 signal (signal unit) was significantly lower in iNPH cases at various locations in pons, thalamus, periventricular frontal horn, and IFG. In iNPH cases, the change was significantly higher in periventricular frontal horn and IFG between last daytime exam and at 24 h (Supplementary Table 3), and remained at a higher level after 24 h, indicative of delayed clearance. Reference subjects (Ref): continuous lines; iNPH patients: dotted lines. Differences between groups at individual time points were determined by independent samples t-test (*$P < 0.05$, **$P < 0.01$, ***$P < 0.001$).

after injection of contrast agent through the final MRI examination at Day 1. The tracer did primarily not distribute freely around the brain convexities, but rather within sulci and cisternal spaces traversed by the three major cerebral leptomeningeal arteries (anterior, middle and posterior), and gadobutrol propagated further along their antegrade directions. This distribution pattern in the subarachnoid space could possibly correspond to leptomeningeal perivascular sheaths described in electron microscopy studies (Weller, 2005). In the current *in vivo* observations, MRI demonstrated, however, presence of gadobutrol tracer

around sulcal vessels at a much wider zone (Fig. 3) than can be appreciated by the area covered with an electron microscope. Additional causes to this perivascular distribution pattern should therefore be explored in further studies.

Arterial pulsations are the force behind CSF pulsations (Greitz, 2004). The finding of parenchymal enhancement was strongly correlated with enhancement in adjacent subarachnoid space (Fig. 5), and therefore also strongly supports antegrade CSF flow within paravascular spaces of brain parenchymal penetrating arteries. This is consistent with animal studies where tracer was administered in
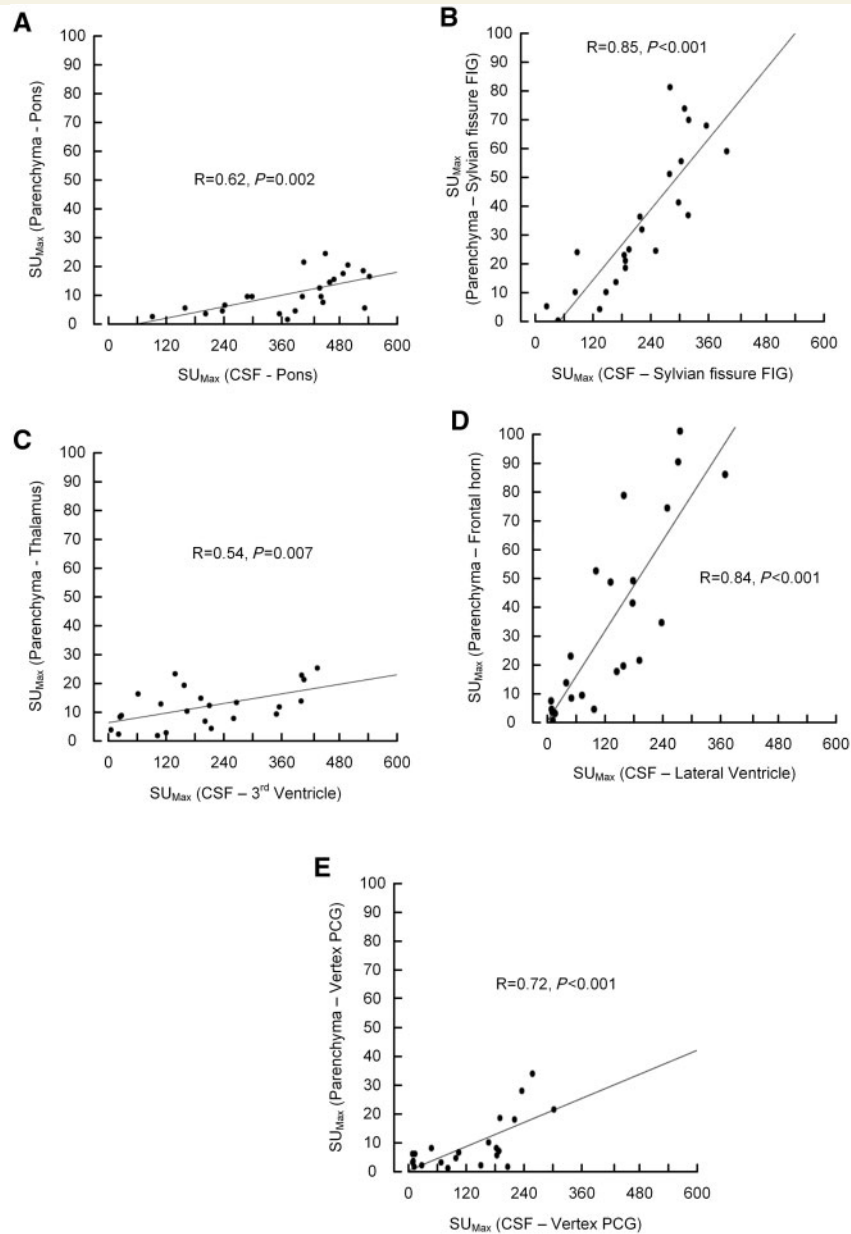
Figure 5 Glymphatic enhancement as function of CSF enhancement. The association between maximum enhancement within the CSF spaces and nearby brain parenchyma was determined for different regions of interest. For all locations (**A–E**), there was a highly significant correlation between contrast agent availability within the CSF space and enhancement of gadobutrol within nearby parenchyma.

Table 2 Information about the clearance phase for different regions of interest within CSF and venous spaces

Clearance phase	Clearance time (min)		Max reduction (SU)		Clearance coefficient (SU/min)	
	iNPH	REF	iNPH	REF	iNPH	REF
CSF space						
Foramen magnum	1264.3 ± 116.1	1294.4 ± 154.5	−206.7 ± 90.8[b]	−358.1 ± 117.7	−0.16 ± 0.07 [b]	−0.28 ± 0.08
Sylvian fissure	1123.7 ± 41.1	1162.6 ± 78.1	−68.0 ± 51.2[a]	−133.0 ± 68.4	−0.06 ± 0.05[a]	−0.12 ± 0.06
Pontine cistern	1207.9 ± 114.8	1261.5 ± 137.0	−177.9 ± 95.5[b]	−313.3 ± 105.3	−0.15 ± 0.08[b]	−0.25 ± 0.08
Fourth ventricle	1234.4 ± 109.1	1287.6 ± 105.9	−231.6 ± 128.1	−232.6 ± 103.7	−0.19 ± 0.1	−0.18 ± 0.08
Third ventricle	1234.3 ± 116.2	1135.3 ± 74.2	−114.4 ± 76.8	−103.7 ± 83.9	−0.10 ± 0.07	−0.09 ± 0.08
Lateral Ventricle	1115.1 ± 46.3	1098.0 ± 12.5	−57.3 ± 48.9	−72.3 ± 11.9	−0.05 ± 0.04	−0.07 ± 0.01
Precentral sulcus	1375.5 + 67.2	1261.7 + 168.6	−6.5 + 3.5	−57.0 + 63.2	−0.005 + 0.003	−0.05 + 0.06
Central venous space						
Sagittal sinus/confluence	1287.4 ± 150.9	1247.3 ± 175.9	−12.1 ± 6.7	−9.5 ± 3.9	−0.01 ± 0.006	−0.008 ± 0.003

Significant differences between iNPH and REF groups were determined by independent samples *t*-test: [a]$P < 0.05$, [b]$P < 0.01$, [c]$P < 0.001$.
REF = reference subject; SU = signal unit.
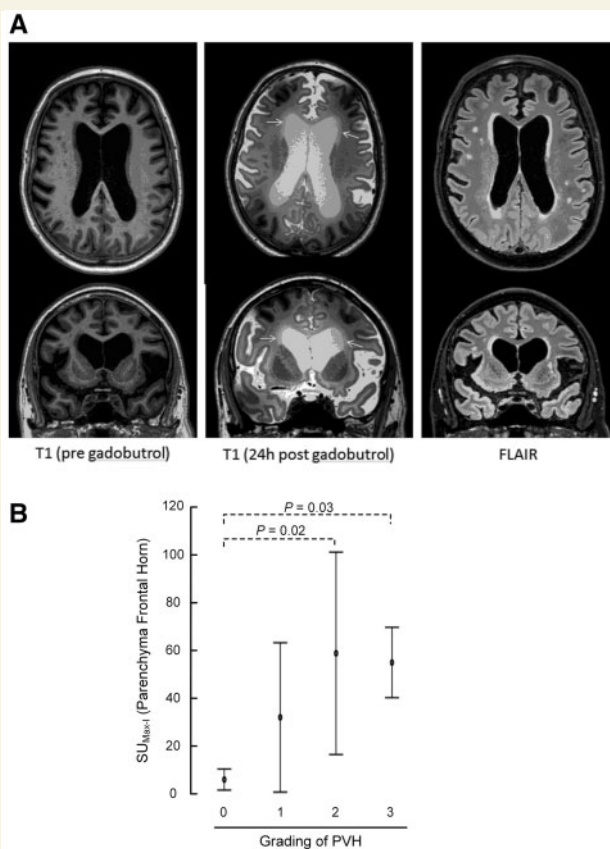
Figure 6 Transependymal flow of MRI contrast agent.
(**A**) Periventricular hyperintensity (PVH) was identified and graded into four grades from FLAIR images (*right column*). The maximum increase in signal unit within the periventricular brain parenchyma between pre-contrast MRI (*left column*) and 24 h post-contrast MRI (*middle column*) was related to the periventricular hyperintensity categories. *Top row*: Axial sections; *bottom row*: coronal sections. (**B**) ANOVA with Bonferroni corrected *post hoc* tests revealed that periventricular enhancement was significantly larger in periventricular lucency grades 2 and 3 than grade 0.

subarachnoid space (Iliff *et al.*, 2012, 2013*a*; Bedussi *et al.*, 2017), but contradictory to studies where intraparenchymal injection of tracers has been used (Carare *et al.*, 2008; Bakker *et al.*, 2016), where it was concluded with retrograde flow. Presence of soluble amyloid-β deposits in the walls of leptomeningeal arteries has previously led to the conclusion that CSF and solutes exit the brain along arteries (Weller *et al.*, 2009). It has, however, been proposed that different directions of CSF flow along paravascular pathways may co-exist (Bakker *et al.*, 2016). While we found evidence for antegrade periarterial movement of the CSF tracer, there was in many iNPH and reference subjects, a strikingly sparse and sometimes absent enhancement of tracer at the upper brain convexities, even after 24 h with patients remaining mainly in the supine position. One explanation to these observations might be a gradient of net CSF flow from the upper towards the lower brain convexities, suggesting CSF secretion at the upper brain

convexities and thus a very limited role of arachnoid villi along the sagittal sinus for CSF resorption. While CSF seems to enter the brain driven by high-pressure arteries traversing the lower surface of the brain, it could be hypothesized that CSF exits at paravenous routes mainly along areas of the brain where presence of (and translated pressure from) larger arteries is more sparse, which is the case around the upper convexities.

In iNPH, reduced intracranial compliance and increased intracranial pulse pressure is an important feature of the disease (Eide and Sorteberg, 2010), and it has also been described as a 'restricted arterial pressure pulsation syndrome' (Greitz, 2004), referring to decreased ability of arteries in subarachnoid space to expand secondary to reduced intracranial compliance. In mice, it was demonstrated that decreased arterial pulsatility reduced paravascular flow (Iliff *et al.*, 2013*b*). In our cohort of iNPH patients with expected decreased arterial pulsatility due to reduced intracranial compliance, and consistent with the mentioned observations in mice, we found that the gadobutrol tracer distributed more slowly along external brain surface arteries than in reference subjects, and further, clearance of gadobutrol was decreased. It may therefore be hypothesized that a vicious cycle may be established in iNPH, where restricted arterial pulsations reduces glymphatic flow, which leads to reduced transport of CSF and solutes through glymphatic pathways and thereby further reduces intracranial compliance. In Alzheimer's disease, the glymphatic system may contribute to a larger portion of extracellular amyloid-β clearance than previously thought (Tarasoff-Conway *et al.*, 2016), and a recent study demonstrated Alzheimer's disease-related biopsy findings in iNPH patients with signs of reduced compliance (Kojoukhova *et al.*, 2017). Reduced intracranial compliance in iNPH may, however, be a phenomenon secondary to obstructed CSF flow. In light of the evolving knowledge of brain glymphatic function, we find it reasonable to attribute delayed propagation and clearance of the CSF tracer gadobutrol, as well as presumed restricted CSF pulsations, to an obstruction of CSF flow between the paravascular and interstitial spaces. Increased resistance to glymphatic flow may also cause CSF to follow pathways of least resistance, among them, the retrograde transventricular route. An obstruction at this level would also explain disproportionate and localized expansion of subarachnoid space around large leptomeningeal arteries in iNPH, which is referred to by some as DESH (disproportionally enlarged subarachnoid-spaces hydrocephalus) (Hashimoto *et al.*, 2010), but not why Virchow-Robin spaces are macroscopically not enlarged (Ishikawa *et al.*, 2015).

Astrocytic end feet enclose all parenchymal brain vessels, and the water channel AQP4 occupies up to 40% of the end foot area, rendering a vast surface for water transport throughout the entire brain (Nagelhus and Ottersen, 2013). While it has been demonstrated that glymphatic function and clearance of metabolites from the extracellular space is reduced in AQP4 knock-out mice (Iliff *et al.*, 2012), no

studies have yet been published regarding AQP4 function in iNPH. In idiopathic intracranial hypertension perivascular AQP4 was, however, increased, and it was interpreted as a possible compensatory mechanism to enhance brain fluid drainage (Eide *et al.*, 2016). We expect upcoming studies of AQP4 content, function and polarization in iNPH patients.

Ventricular reflux of gadobutrol in idiopathic normal pressure hydrocephalus

In iNPH, gadobutrol entered the ventricular system early, remained in the ventricles over time, and correlated strongly with contrast enhancement in adjacent periventricular white matter, indicating transependymal migration of the contrast agent, which in its turn was associated with periventricular hyperintensity at FLAIR images. These observations support previous findings of net retrograde aqueductal flow in iNPH (Ringstad *et al.*, 2016; Yin *et al.*, 2017), and this phenomenon has also been associated with restricted intracranial pulsations and change of net flow in the antegrade direction after surgical shunting (Ringstad *et al.*, 2016). Aqueductal net flow is typically reported in microlitres, which might be within the range of measurement inaccuracies, and has by some been considered a sign of measurement inaccuracy when it is observed, and therefore been subtracted when estimating the more robust parameter aqueductal stroke volume to predict shunt response in NPH (Bradley *et al.*, 1996). Our observations of ventricular reflux might contribute to explain the mechanism behind hydrocephalus in NPH, since a precondition for such flow would be a minute positive pressure gradient from the subarachnoid space to the ventricles, and also over the ventricular ependyma. Ventricular dilatation may therefore constitute a manifestation of how the brain adapts to such a minor pressure gradient, while also increased area of the ependymal surface and stretching of ependymal lining may facilitate transependymal water transport. It seems reasonable to assume that the periventricular gadobutrol enhancement observed in periventricular hyperintensity grade 1–3 expresses transependymal migration by the same mechanisms as reported in previous studies (Bering and Sato, 1963; Sahar *et al.*, 1969) rather than within the traditional defined glymphatic pathway via periarterial spaces. A transependymal pressure gradient, even small, may be sufficient to enlarge the ventricles (Linninger *et al.*, 2005; Levine, 2008). In one study with invasive monitoring, the pulse pressure amplitude was median 0.4 mm Hg higher inside the ventricles than in the parenchyma (Eide, 2008). Another study was, however, not able to measure a transependymal pressure gradient (Eide and Saehle, 2010).

Brain enhancement and clearance of gadobutrol

Before glymphatic contrast enhancement, the parenchymal T_1 signal unit was lower in all regions of interest in iNPH compared to reference subjects. We attribute this to an increase in brain water content in iNPH, since water is by far the most significant contributor to prolonged T_1 relaxation in the brain. Signs of increased brain water content in NPH has also previously been demonstrated in several brain regions by using MRI diffusion-weighted imaging (Gideon *et al.*, 1994). In light of the previously discussed potential role of AQP4, it is notable that increased brain water content is also seen in mice with complete loss of AQP4, however, not in mice with selective removal of perivascular AQP4 or deletion of ependymal AQP4 (Vindedal *et al.*, 2016).

Glymphatic enhancement was observed at all locations when preceded by enhancement of the adjacent subarachnoid space, but was not observed in every patient at all locations, and there were substantial interindividual variations (Supplementary Table 2). The current study does not fully reveal why such differences exist, but we notice that glymphatic enhancement was particularly apparent and frequent at the inferior frontal gyrus in both iNPH and reference subjects, which anatomically is adjacent to the middle cerebral artery, consistent with a fundamental role of pulsations for glymphatic transport, as mentioned. Interestingly, this current *in vivo* observation is contradictory to recent modelling studies, which conclude that arterial pulsations are an unlikely origin of the driving force that could account for convective solute transport through the interstitial space (Asgari *et al.*, 2016; Jin *et al.*, 2016).

In contradiction to previous data from anaesthetized mice and rats, where glymphatic enhancement typically peaked within 2 h, glymphatic enhancement in humans peaked at 24 h, and was, except from in periventricular white matter in iNPH, not detectable at MRI exams obtained at first-day time intervals following administration of the intrathecal tracer (Fig. 4). Xie *et al.* (2013) demonstrated that natural sleep or anaesthesia is associated with a 60% increase in the interstitial space, which increased glymphatic clearance of amyloid-β 2-fold. Our observations indicate that glymphatic function is also highly dependent on sleep in humans.

While enhancement peaked at the final MRI exam of the study protocol, clearance of gadobutrol from brain parenchyma could not be calculated, and further studies should account for this observation. However, as clearance of gadobutrol was delayed in CSF, and glymphatic enhancement was found to be a function of CSF enhancement (Fig. 5), we find it reasonable to hypothesize that maximum parenchymal enhancement at 24 h is a sign of reduced clearance of gadobutrol via the glymphatic system in iNPH. As failure of glymphatic function has previously been associated with reduced clearance of interstitial solutes like amyloid-β, it seems reasonable to hypothesize that the previously poorly understood iNPH dementia may share a pathogenic mechanism with Alzheimer's disease.

There were no signs of contrast agent enhancement at the venous side (superior sagittal sinus) at any time point, indicating no effect on other observations due to circulating

contrast agent in veins. The image resolution of a 3 T human study is insufficient to allow for detection of meningeal lymphatic vessels that have previously been proposed to represent potential drainage routes from the glymphatic circulation (Louveau *et al.*, 2015).

Limitations

CSF leakage was diagnosed in 2/8 reference subjects. These reference subjects may therefore not have a normal CSF flow pattern, and intracranial hypotension may be assumed to affect paravascular transport as well, given the important role of CSF pulsations. However, there was no obvious difference in T_1 signal unit change (glymphatic enhancement) in the two patients with leakage compared to the reference subject group. A second limitation is that reference subjects were significantly younger than the iNPH patients and of different gender. It can therefore not be established to what degree iNPH disease or age/gender contributed to differences between groups, while reduced glymphatic function should be expected with normal ageing (Kress *et al.*, 2014). However, in addition to the observed signs of different glymphatic clearance between the two groups, there are also substantial differences in speed of gadobutrol propagation in CSF as well as ventricular reflux pattern, which may less likely represent age effects. We therefore hypothesize that signs of glymphatic impairment in the iNPH group are more likely to be disease-specific rather than purely due to the patient'sage.

Moreover, even though we standardized MRI routines extensively, imaging time points after contrast agent injection were not identical due to practical limitations, and MRI exams were therefore rather categorized at defined time intervals. We did not think it reasonable to enforce restrictions on patient movement between the final MRI of Day 1 and the MRI of following morning, and could therefore not control data for patient activity and body position during that time period, nor for sleep. In these cohorts of symptomatic patients, already burdened with an extensive number of imaging procedures, it was considered unreasonable, and even unethical, to demand further exams during evening or night-time. However, this also represents a weakness of the study, as it cannot be established at which exact time point glymphatic enhancement first occurred. The hypothesis that sleep might have an impact on glymphatic function may still be sustained by observations of no, or very sparse, parenchymal enhancement during Day 1, in spite of an adequate amount of contrast agent at the adjacent brain surface, but enhancement at MRI performed on the morning of Day 2 (24 h).

Finally, MRI analysis of signal unit at different time points was carried out manually from predefined areas of brain and CSF spaces, where regions of interest had to be fitted to adjust for local anatomy to avoid partial volume averaging effect. In future studies, a whole-brain and -CSF approach should be preferred. This would require perfect alignment and co-registration of images from different time points, as well as segmentation techniques to differentiate brain subregions, and CSF from parenchyma. We are in the process of elaborating such postprocessing algorithms with external partners.

Conclusion

Intrathecal administration of an MRI contrast agent (gadobutrol) serving as CSF tracer, followed by multiple MRI exams over 24 h (glymphatic MRI), demonstrated signs of delayed glymphatic clearance in iNPH patients compared with a reference group. In all study subjects, the CSF tracer propagated in the subarachnoid space antegradely along large leptomeningeal arteries, and presence of tracer in subarachnoid space always preceded glymphatic enhancement in adjacent brain tissue, indicating a pivotal role of intracranial pulsations for glymphatic function. Glymphatic enhancement peaked overnight, and we attribute this to increased glymphatic function during sleep, which has been suggested in previous animal experiments. The sparse enhancement of CSF tracer at the upper brain convexities in both study cohorts questions the role of CSF resorption at the arachnoid villi. Other features of iNPH were ventricular reflux and transependymal migration of the tracer from the lateral ventricles towards the brain parenchyma. Given the ability of MRI contrast agents to access and be cleared from the brain extravascular space after intrathecal administration, glymphatic MRI may have the potential to assess brain metabolic function.

Acknowledgements

Funding

Supplementary material

Supplementary material is available at *Brain* online.

References

Adams RD, Fisher CM, Hakim S, Ojemann RG, Sweet WH. Symptomatic occult hydrocephalus with "Normal" cerebrospinal-fluid pressure. A treatable syndrome. N Eng J Med 1965; 273: 117–26.

Akbar JJ, Luetmer PH, Schwartz KM, Hunt CH, Diehn FE, Eckel LJ. The role of MR myelography with intrathecal gadolinium in localization of spinal CSF leaks in patients with spontaneous intracranial hypotension. AJNR Am J Neuroradiol 2012; 33: 535–40.

Asgari M, de Zelicourt D, Kurtcuoglu V. Glymphatic solute transport does not require bulk flow. Sci Rep 2016; 6: 38635.

Aydin K, Guven K, Sencer S, Jinkins JR, Minareci O. MRI cisternography with gadolinium-containing contrast medium: its role, advantages and limitations in the investigation of rhinorrhoea. Neuroradiology 2004; 46: 75–80.

Bakker EN, Bacskai BJ, Arbel-Ornath M, Aldea R, Bedussi B, Morris AW, et al. Lymphatic clearance of the brain: perivascular, paravascular and significance for neurodegenerative diseases. Cell Mol Neurobiol 2016; 36: 181–94.

Bedussi B, van der Wel NN, de Vos J, van Veen H, Siebes M, VanBavel E, et al. Paravascular channels, cisterns, and the subarachnoid space in the rat brain: a single compartment with preferential pathways. J Cereb Blood Flow Metab 2017; 37: 1374–85.

Bering EA Jr, Sato O. Hydrocephalus: changes in formation and absorption of cerebrospinal fluid within the cerebral ventricles. J Neurosurg 1963; 20: 1050–63.

Bradley WG Jr, Scalzo D, Queralt J, Nitz WN, Atkinson DJ, Wong P. Normal-pressure hydrocephalus: evaluation with cerebrospinal fluid flow measurements at MR imaging. Radiology 1996; 198: 523–9.

Cabral D, Beach TG, Vedders L, Sue LI, Jacobson S, Myers K, et al. Frequency of Alzheimer's disease pathology at autopsy in patients with clinical normal pressure hydrocephalus. Alzheimers Dement 2011; 7: 509–13.

Carare RO, Bernardes-Silva M, Newman TA, Page AM, Nicoll JA, Perry VH, et al. Solutes, but not cells, drain from the brain parenchyma along basement membranes of capillaries and arteries: significance for cerebral amyloid angiopathy and neuroimmunology. Neuropathol Appl Neurobiol 2008; 34: 131–44.

Cheng KT. Gadobutrol. Molecular Imaging and Contrast Agent Database (MICAD). Bethesda, MD: National Center for Biotechnology Information (US); 2004.

Eide PK. Demonstration of uneven distribution of intracranial pulsatility in hydrocephalus patients. J Neurosurg 2008; 109: 912–17.

Eide PK, Eidsvaag VA, Nagelhus EA, Hansson HA. Cortical astrogliosis and increased perivascular aquaporin-4 in idiopathic intracranial hypertension. Brain Res 2016; 1644: 161–75.

Eide PK, Ringstad G. MRI with intrathecal MRI gadolinium contrast medium administration: a possible method to assess glymphatic function in human brain. Acta Radiol Open 2015; 4: 2058460115609635.

Eide PK, Saehle T. Is ventriculomegaly in idiopathic normal pressure hydrocephalus associated with a transmantle gradient in pulsatile intracranial pressure? Acta Neurochir 2010; 152: 989–95.

Eide PK, Sorteberg W. Diagnostic intracranial pressure monitoring and surgical management in idiopathic normal pressure hydrocephalus: a 6-year review of 214 patients. Neurosurgery 2010; 66: 80–91.

Gideon P, Thomsen C, Gjerris F, Sorensen PS, Henriksen O. Increased self-diffusion of brain water in hydrocephalus measured by MR imaging. Acta Radiol 1994; 35: 514–19.

Greitz D. Radiological assessment of hydrocephalus: new theories and implications for therapy. Neurosurg Rev 2004; 27: 145–65; discussion 166–7.

Hashimoto M, Ishikawa M, Mori E, Kuwana N. Diagnosis of idiopathic normal pressure hydrocephalus is supported by MRI-based scheme: a prospective cohort study. Cerebrospinal Fluid Res 2010; 7: 18.

Heinz ER, Davis DO, Karp HR. Abnormal isotope cisternography in sympatomatic occult hydrocephalus. A correlative isotopic-neuroradiological study in 130 subjects. Radiology 1970; 95: 109–20.

Hladky SB, Barrand MA. Mechanisms of fluid movement into, through and out of the brain: evaluation of the evidence. Fluids Barriers CNS 2014; 11: 26.

Iliff JJ, Lee H, Yu M, Feng T, Logan J, Nedergaard M, et al. Brain-wide pathway for waste clearance captured by contrast-enhanced MRI. J Clin Invest 2013a; 123: 1299–309.

Iliff JJ, Wang M, Liao Y, Plogg BA, Peng W, Gundersen GA, et al. A paravascular pathway facilitates CSF flow through the brain parenchyma and the clearance of interstitial solutes, including amyloid beta. Sci Transl Med 2012; 4: 147ra111.

Iliff JJ, Wang M, Zeppenfeld DM, Venkataraman A, Plog BA, Liao Y, et al. Cerebral arterial pulsation drives paravascular CSF-interstitial fluid exchange in the murine brain. J Neurosci 2013b; 33: 18190–9.

Ishikawa M, Yamada S, Yamamoto K. Three-dimensional observation of Virchow-Robin spaces in the basal ganglia and white matter and their relevance to idiopathic normal pressure hydrocephalus. Fluids Barriers CNS 2015; 12: 15.

Iwamoto T, Miyaji H, Kanaya K, Takasaki M. Periventricular lucency evaluated by second-derivative finger plethysmography. Geriatr Gerontol Int 2001; 1: 25–32.

Jessen NA, Munk AS, Lundgaard I, Nedergaard M. The glymphatic system: a beginner's guide. Neurochem Res 2015; 40: 2583–99.

Jin BJ, Smith AJ, Verkman AS. Spatial model of convective solute transport in brain extracellular space does not support a "glymphatic" mechanism. J Gen Physiol 2016; 148: 489–501.

Jinkins JR, Rudwan M, Krumina G, Tali ET. Intrathecal gadolinium-enhanced MR cisternography in the evaluation of clinically suspected cerebrospinal fluid rhinorrhea in humans: early experience. Radiology 2002; 222: 555–9.

Kojoukhova M, Vanha KI, Timonen M, Koivisto AM, Nerg O, Rummukainen J, et al. Associations of intracranial pressure with brain biopsy, radiological findings, and shunt surgery outcome in patients with suspected idiopathic normal pressure hydrocephalus. Acta Neurochir 2017; 159: 51–61.

Kress BT, Iliff JJ, Xia M, Wang M, Wei HS, Zeppenfeld D, et al. Impairment of paravascular clearance pathways in the aging brain. Ann Neurol 2014; 76: 845–61.

Lee H, Xie L, Yu M, Kang H, Feng T, Deane R, et al. The effect of body posture on brain glymphatic transport. J Neurosci 2015; 35: 11034–44.

Levine DN. Intracranial pressure and ventricular expansion in hydrocephalus: have we been asking the wrong question? J Neurol Sci 2008; 269: 1–11.

Linninger AA, Tsakiris C, Zhu DC, Xenos M, Roycewicz P, Danziger Z, et al. Pulsatile cerebrospinal fluid dynamics in the human brain. IEEE Trans Biomed Eng 2005; 52: 557–65.

Lohrke J, Frenzel T, Endrikat J, Alves FC, Grist TM, Law M, et al. 25 years of contrast-enhanced MRI: developments, current challenges and future perspectives. Adv Ther 2016; 33: 1–28.

Louveau A, Smirnov I, Keyes TJ, Eccles JD, Rouhani SJ, Peske JD, et al. Structural and functional features of central nervous system lymphatic vessels. Nature 2015; 523: 337–41.

Malayeri AA, Brooks KM, Bryant LH, Evers R, Kumar P, Reich DS, et al. National Institutes of Health perspective on reports of gadolinium deposition in the brain. J Am Coll Radiol 2016; 13: 237–41.

Nagelhus EA, Ottersen OP. Physiological roles of aquaporin-4 in brain. Physiol Rev 2013; 93: 1543–62.

Penn RD, Basati S, Sweetman B, Guo X, Linninger A. Ventricle wall movements and cerebrospinal fluid flow in hydrocephalus. J Neurosurg 2011; 115: 159–64.

Plog BA, Dashnaw ML, Hitomi E, Peng W, Liao Y, Lou N, et al. Biomarkers of traumatic injury are transported from brain to blood via the glymphatic system. J Neurosci 2015; 35: 518–26.

Reiche W, Komenda Y, Schick B, Grunwald I, Steudel WI, Reith W. MR cisternography after intrathecal Gd-DTPA application. Eur Radiol 2002; 12: 2943–9.

Ringstad G, Emblem KE, Eide PK. Phase-contrast magnetic resonance imaging reveals net retrograde aqueductal flow in idiopathic normal pressure hydrocephalus. J Neurosurg 2016; 124: 1850–7.

Sahar A, Hochwald GM, Ransohoff J. Alternate pathway for cerebrospinal fluid absorption in animals with experimental obstructive hydrocephalus. Exp Neurol 1969; 25: 200–6.

Tarasoff-Conway JM, Carare RO, Osorio RS, Glodzik L, Butler T, Fieremans E, et al. Clearance systems in the brain–implications for Alzheimer diseaser. Nat Rev Neurol 2016; 12: 248.

van Swieten JC, Hijdra A, Koudstaal PJ, van Gijn J. Grading white matter lesions on CT and MRI: a simple scale. J Neurol Neurosurg Psychiatry 1990; 53: 1080–3.

Vindedal GF, Thoren AE, Jensen V, Klungland A, Zhang Y, Holtzman MJ, et al. Removal of aquaporin-4 from glial and ependymal membranes causes brain water accumulation. Mol Cell Neurosci 2016; 77: 47–52.

Weller RO. Microscopic morphology and histology of the human meninges. Morphologie 2005; 89: 22–34.

Weller RO, Boche D, Nicoll JA. Microvasculature changes and cerebral amyloid angiopathy in Alzheimer's disease and their potential impact on therapy. Acta Neuropathol 2009; 118: 87–102.

Xie L, Kang H, Xu Q, Chen MJ, Liao Y, Thiyagarajan M, et al. Sleep drives metabolite clearance from the adult brain. Science 2013; 342: 373–7.

Yang L, Kress BT, Weber HJ, Thiyagarajan M, Wang B, Deane R, et al. Evaluating glymphatic pathway function utilizing clinically relevant intrathecal infusion of CSF tracer. J Transl Med 2013; 11: 107.

Yin LK, Zheng JJ, Zhao L, Hao XZ, Zhang XX, Tian JQ, et al. Reversed aqueductal cerebrospinal fluid net flow in idiopathic normal pressure hydrocephalus. Acta Neurol Scand 2017. [Epub ahead of print]. doi: 10.1111/ane.12750.